Available online at www.sciencedirect.com
ScienceDirect
Journal of the European Ceramic Society 32 (2012) 307–315
www.elsevier.com/locate/jeurceramsoc

Calcium oxides for CO_2 capture obtained from the thermal decomposition of $CaCO_3$ particles coprecipitated with Al^{3+} ions

D.T. Beruto [b,a,*], R. Botter [b,a], A. Lagazzo [a], E. Finocchio [a]

[a] *Department of Chemical Engineering and Processing, Faculty of Engineering, University of Genoa, P.le J.F. Kennedy (Fiera del Mare), Pad. D, 16129 Genoa, Italy*
[b] *Research Centre for Materials Science and Eng., University of Genoa, Italy*

Received 20 April 2011; received in revised form 1 August 2011; accepted 7 August 2011
Available online 3 September 2011

Abstract

Calcium-carbonate powders were coprecipitated with Al^{3+} and then decomposed in air and/or under a CO_2 flux between 590 °C and 1150 °C. The data were analysed using a consecutive-decomposition-dilatometer method and the kinetic results were discussed according to the microstructure analysis done by N_2 adsorption isotherms (78 K), SEM and FT-IR measurements. Below 1000 °C, $CaCO_3$ particle thermal-decomposition was pseudomorphic, resulting in the formation of a CaO grain porous network. When the CaO grains were formed, the Al^{3+} diffused among them, producing AlO_4 groups that promoted the CaO grain coarsening and reduced O^{2-} surface sites available to CO_2 adsorbed molecules to form CO_3^{2-}. In pure CaO, CO_3^{2-} diffused through the grain boundary, enhancing Ca^{2+} and O^{2-} mobility; AlO_4 groups reduced CO_3^{2-} penetration and CaO sintering rate. Above 1000 °C, the sintering rate of the doped samples exceeded that of the undoped, likely because of Al^{3+} diffusion in CaO and viscous flow.
© 2011 Elsevier Ltd. All rights reserved.

Keywords: Limestone decomposition; Sintering; CO_2 capture; Al ions; Dilatometer

1. Introduction

The separation of CO_2 from flue gases using conventional air-blown combustion systems and the storage of CO_2-rich gases in underground geological formation or in the deep ocean are approaches suggested for reducing the greenhouse effect of CO_2. Among the separation processes, the carbonate looping process for postcombustion CO_2 capture appears to be a promising technology.[1–4] This method involves the use of a fluidised bed where lime reacts with a fuel gas and another fluidised bed, the calciner, where the adsorbent is regenerated and pure CO_2 is produced. The choice of natural limestone as the CO_2 carrier is an attractive option because it is a cheap and abundant material with large and important applications in steel making,[5,6] building, cultural heritage,[7] and environmental applications.[8–10]

Regarding CO_2 capture technology, the porous lime particles obtained from the thermal decomposition of limestone need to have high efficiency in CO_2 capture and the capacity to endure a high number of carbonate looping cycles.

This requires that the porous calcium oxide particles obtained in the calciner are characterised by optimal and stable values for surface area, porosity and pore shape for the subsequent CO_2 adsorption from the flue gases. Because both fluidised beds are in air and in CO_2 flux, the surface area and porosity values of high surface porous calcium oxide (CaO) particles are rapidly reduced due to the temperature and catalytic effect of CO_2 on CaO sintering.[11–13]

For these reasons, CaO obtained from the thermal decomposition of limestone particles in air/CO_2 environments is characterised by surface area values of approximately $1 \times 10\ m^2/g$. Although the sintering of these oxides in CO_2 proceeds extremely slowly,[12] it has been found that the surface and porosity values of CaO-adsorbent particles obtained from calciners are reduced after a large number of cycles.[14,15]

Regarding new lime adsorbents with enhanced durability, previous studies[16–24] reported promising materials with a reasonable stable uptake of CO_2 obtained by mixing CaO on the

* Corresponding author at: Research Centre for Materials Science and Eng., University of Genoa, 16129 Genova, GE, Italy. Tel.: +39 010 353 6039; fax: +39 010 353 6034.
E-mail address: dabe@unige.it (D.T. Beruto).

0955-2219/$ – see front matter © 2011 Elsevier Ltd. All rights reserved.
doi:10.1016/j.jeurceramsoc.2011.08.022

molecular level with an inert supporting material with a high melting point, such as Al_2O_3, MgO or TiO_2. Improvements in obtaining these adsorbents have been made[25] by using CaO coprecipitation and hydrolysis methods.

Despite the promising results obtained by testing these materials in pilot plants, according to the opinion of the authors, the mechanism explaining how and why the uptake of CO_2 by these materials is more efficient than that of CaO obtained by the thermal decomposition of limestone/calcium carbonate particles remains to be elucidated.

This is not surprising because, as far as we are aware, the ultimate mechanism by which CO_2 catalyses the sintering of CaO has not been established.

In this paper, we concentrate our efforts on explaining this mechanism by using $CaCO_3$ particles precipitated from $CaCl_2{\cdot}2H_2O$ solutions in the presence and absence of $AlCl_3{\cdot}6H_2O$ salts as starting materials.

The background for this study is derived from previous experimental findings[12,26,27] of the sintering effects of gases such as CO_2 and H_2O on CaO and MgO.

In one of those papers,[27] we stated that any gas used as a catalyst for the sintering of a solid oxide must be chemically adsorbed to the surface of the oxide surface and then it must penetrate into the oxide in its bulk phases.

The experiments designed in this paper will prove that the above statement holds when CaO in the presence and absence of Al^{3+} ions is exposed to CO_2 in the temperature range of 590–1000 °C. Thus, the rule that CO_2 and H_2O must diffuse as CO_3^{2-} and OH^- ions, respectively, into the oxide through grain boundary paths to be effective catalysts will be applied as a solid scientific basis to understand how and why ions smaller than Ca^{2+} can be used to stabilise the surface area and porosity of new CO_2 adsorbents in the carbonate looping process.

2. Experimental

2.1. Materials

The starting materials were $CaCl_2{\cdot}2H_2O$, $AlCl_3{\cdot}6H_2O$, 33% ammonia (NH_3) solution (each from Sigma–Aldrich), and 99.999% CO_2 gas (Air Liquide).

All inorganic chemicals were used without purification. A stock solution of $CaCl_2$ was freshly prepared by adding distilled water to reach the concentration of 1 mol/l. To produce the aluminium-doped $CaCO_3$, another solution was prepared by adding 2.41 g of $AlCl_3{\cdot}6H_2O$ to 1 l of $CaCl_2$ 1 M. Ammonium carbonate solution was prepared bubbling CO_2 into a 2 M NH_3 solution until a pH value of 8.47 was reached. The $CaCO_3$ powder was prepared by adding into the water-jacketed beaker containing 600 ml of the $(NH_4)_2CO_3$ solution and 500 ml of $CaCl_2$ solution. With respect the 1:1 ratio required by the stoichiometric reaction between $(NH_4)_2CO_3$ and $CaCl_2$, the $(NH_4)_2CO_3$ results the 20% greater. The solution was continuously stirred for 20 min, the reaction temperature was kept constant at 25 °C and changes in pH were recorded both for the precipitation without and with $AlCl_3$. A rapid decreasing of the pH down to 6.5 followed by an increasing to pH 8 was observed when $AlCl_3$ is not present, while in the case of doped material, the minimum pH was around 6.2 and the final one was 7.14. The precipitate was aged for 24 h. After sedimentation, the powders were collected and washed with distilled water until chloride ions were completely removed. The chlorine ion concentration in the liquid phase was checked with a 0.1 N $AgNO_3$ solution.

The obtained precipitates were settled by centrifugation and dried at room temperature in a desiccator for 1 week.

2.2. Methods

Cylindrical pellets of 8 ± 0.1 mm in diameter and 7.6 ± 0.1 mm were prepared with an uniaxial cylindrical mould. Due to the importance of the pelletisation step, great care was paid to obtain pellets of doped/not doped calcium carbonate with the same initial density.

230 mg of doped/not doped calcium carbonate powders as they have been obtained after the precipitation process and after the drying step were introduced in stainless cylinder without using lubricants at the wall to avoid contamination.[28] A two steps pressing procedure was adopted. The first step had a stop point at 100 MPa for 2 min, the second one had a maximum value of 195 MPa for further 2 min. Final density of the sample was evaluated trough weight – geometrical volume measurements. The final density of all the sample turned out to be fairly constant and equal to 1.9 ± 0.01 g/cm^3 for both the carbonates. This value corresponds to a relative density of 0.7 compared with the theoretical density of calcite.[29]

2.3. Thermogravimetry (TG)

Dynamic TG measurements were performed in a static air atmosphere using a Netzsch STA 409 equipped with platinum TG-DSC thermal analyser in the sensitivity range of ±0.1 mg and with a Netzsch 410 furnace temperature controller system. It is well known[30] that in dynamic thermal decomposition the actual temperature of the sample might be different from the one actual measured at the time *t*, due to thermal transport phenomena. These transport phenomena are different for pellets and for powders even if the chemical nature is the same. Since in this paper we are interested to the differences in the decomposition between doped and non doped samples, both pellet and powders were heated at 10 °C/min in air. Effects of the heat transport and of crucible height[31] will result by the difference in the decomposition behaviour between the same kind of pellets and powders.

Platinum crucible of 6 mm in diameter and 3 mm in height was used, while the pellet was directly placed on the platinum sample holder. The temperature range between 20 °C and 1200 °C was explored when the furnace was kept in static air atmosphere.

To minimize the transport heat phenomena[32] in decomposition of doped and non doped powders, a "quasi-isothermal" run was made keeping the heating rate at the minimum value that the instrument allows, i.e. 0.1 °C/min and reducing the weight of the loose powder sample to 20 mg to minimize the absorption–desorption phenomena of CO_2 in the powder bed.[33]

The powder samples were placed inside the furnace in a TG-DSC platinum holder (6 mm × 3 mm), and then the temperature was increased from room temperature (approximately 20 ± 1 °C) to 1200 °C at a nominal rate of 10 °C/min, during which time the weight loss and DSC signal were recorded continuously. Pellets were decomposed by placing them directly in the centre of the sample holder without the crucible. Other TG data were acquired using 20 mg of loose powders and a heating rate of 0.1 °C/min.

2.4. Dilatometry

Consecutive decomposition-sintering dilatometer experiments were performed in a Netzsch dilatomer (DIL 402 E) equipped with a furnace identical to the one used in the TG runs and controlled by the same systems. The internal diameter of the DIL 402 E furnace was 26.5 mm, equal to that of the vertical TG-DSC furnace. The pushing rod was alumina (6 mm in diameter) with an added applied force of 0.3 N. $CaCO_3$ pellet cylinders (8 mm in diameter and 8 ± 0.5 mm in length) were introduced into the dilatometer and heated in static air or in CO_2 at a flow rate 48 ± 0.05 ml/min using the same 10 °C/min heating program adopted for the TG experiments. Each run was duplicated with fresh samples to evaluate any statistical deviation. TG traces were reproducible within the instrumental error of 2%, whereas the dilatometer traces were reproducible within the instrumental error of 2–4%. Longitudinal shrinkage was recorded continuously, and radial shrinkage was examined at room temperature and at the end of the experiment at micrometer accuracy (the accuracy was ±0.01 mm). It was noted that the total radial and longitudinal shrinkages were fairly equal within the experimental errors.

Blank runs to calibrate the thermal expansion of the sample holder were done using polycrystalline alumina with a thermal expansion behaviour well characterised and furnished by Netzsch.

Others dilatometer experiments were performed to measure the shrinkage behaviour at constant temperature. These samples were prepared with the following thermal heating program: 10 °C/min up to 950 °C, 8 h at constant temperature, cooling at a nominal rate of 10 °C/min, after 95 min. The temperature decreased at the natural cooling rate of the furnace for approximately 4 h until room temperature was reached. For these runs, the sample holder correction table furnished by Netzsch was used.

2.5. N_2 adsorption isotherms at 78 K

The doped and undoped calcium carbonate powders were placed in an open Pt crucible that was hung from a quartz wire in one chamber of a symmetrical microbalance in a 25-mm diameter quartz resistance furnace that was previously described elsewhere.[26] A nonporous quartz specimen was placed in another Pt crucible in a reference chamber. Double-wound resistance wires were designed to minimize the temperature gradient along the furnace cross section. A chromel–alumel thermocouple tip was placed 5 mm from the bottom of the crucible. Calibration with another thermocouple introduced from the top of the furnace demonstrated that the temperature remained constant within ±1 °C over a length of 5 cm. Decomposition of the calcium carbonate powders was performed in the temperature range of 700–900 °C in air and CO_2 environments.

As soon as the decomposition was complete, without removing the samples, a vacuum was introduced by a system that can pump to approximately 1×10^{-4} Pa at 100 °C for 30 min. Then, the system was cooled down to 78 K, and purified gaseous N_2 was introduced to measure the correspondent adsorption–desorption isotherms.[12] For the sake of comparison, the CaO samples obtained from the dilatometer under the same decomposition-sintering conditions were transported, as fast as possible, from the dilatometer to the symmetrical thermobalance for N_2 adsorption–desorption measurements at 78 K.

2.6. CO_2 high-temperature equilibrium isotherms

The doped and undoped CaO samples obtained in the symmetrical thermobalance with a specific surfaces ranging between 11 and 12.5 m^2/g that did not change significantly during adsorption were exposed to CO_2 for adsorption studies.

Standard tables[34] give an equilibrium calcium carbonate decomposition pressure of 5434 Pa at 720 °C. Isothermal adsorption equilibrium curves were studied in the pressure range of 65 Pa to 98% of the measured equilibrium calcite pressure, which was 5300 Pa. Pressure was controlled by a single-side absolute sensor head and a control system placed at the top of the thermobalance. Weight variations were recorded continuously by using the microbalance with a sensitivity of 2×10^{-5} g/min.

Runs with CO_2 but without samples were performed to calibrate the systems. The sample volume was small so that the value of the pressure inside the thermobalance was not affected by it. Blank runs with N_2 gave buoyancy corrections of 1×10^{-4} g when the pressure was 65 Pa and less than 2×10^{-5} g when the pressure was greater than 150 Pa.

As soon as the samples reached the desired temperature, a CO_2 flow was started. To obtain an equilibrium isotherm, CaO was heated under vacuum and held in CO_2 at the maximum desired pressure below the equilibrium pressure until the weight of the samples was constant for 30 min at the sensitivity of 2×10^{-5} g/min. The pressure was decreased in steps, and the point where the weight changes were constant was considered the equilibrium pressure. After each isotherm, the sample was pumped under vacuum until the initial sample weight was recorded.

To determine the reversibility of the isotherm for some samples, the pressure was increased by the same step increments, and the constant weights reached were reproducible in adsorption and desorption.

2.7. FT-IR measurements

For both doped and undoped samples, pure powder disks of approximately 20 mg were outgassed at 400 °C under high vacuum in the IR cell connected to a conventional gas manipulation apparatus.

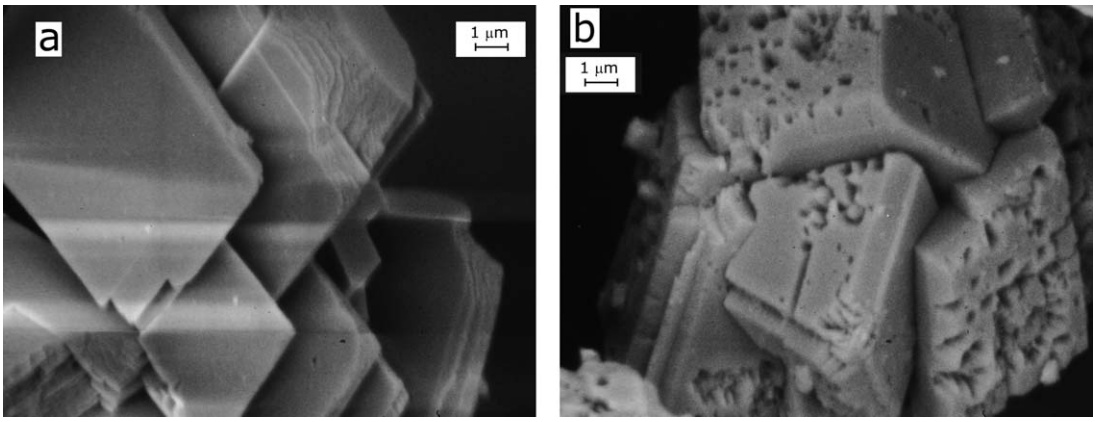

Fig. 1. SEM images (5500×) of typical powders obtained from the precipitation processes of calcium carbonate either undoped (a) or doped (b) with aluminium ions.

IR spectra were recorded by a Nexus Thermonicolet FT instrument (100 scans, DTGS KBr detector, OMINC software).

Skeletal spectra were recorded following dilution of the oxide powders in KBr (1%, w/w) in air.

2.8. SEM

SEM observations were made on the initial doped and undoped calcium carbonate powders and on the final CaO obtained from powders and pellet decomposition-sintering processes in air and CO_2. To minimize possible hydration, the samples were kept in desiccators, and fresh internal fractured surfaces were exposed and coated as soon as they were formed with a layer of gold ~30 nm thick.

3. Results and discussion

Fig. 1(a and b) illustrates the typical powders obtained from the precipitation processes of calcium carbonate either undoped (a) or doped (b) with aluminium ions.

For the sake of clarity, undoped powders were demarcated by 'C', and doped powders were demarcated by 'CD'.

At 5500× magnification, image a shows that the C particles had shapes resembling small calcite crystals[35] with diameters as large as 10 μm. At the same magnification, image b shows that the general shape of the CD particles remained rhombohedral, but some external surfaces large and irregular cavities with diameters as large as 5 μm were present. Very reasonably these features are linked with the different pH kinetics in presence and in absence of the $AlCl_3$.

A new study to evaluate how much Al^{3+} ions can be incorporate in the structure is in progress in our laboratory, at the moment we cannot comment about the final composition of the precipitate.[36]

Fig. 2 shows typical dynamic TG traces of loose C and CD powders and of their corresponding pellets exhibiting an apparent density of 1.89–1.91 g/cm^3 and decomposed in air and at a heating rate of 10 °C/min. From these data the kinetic of decomposition of the powder system are faster than those of the pellet ones. Furthermore it should be observed that the comparison of doped and not doped pellets leads to almost equal kinetics, while the one between doped and non doped powders reads a kinetic of decomposition slightly faster for the not doped system.

The actual internal decomposition temperature of the material inside the pellet is less than that of the one inside of the powder bed due to heat transport phenomena. This makes the pellet kinetic rate lower than the powder one. Furthermore and even more important, the diffusion path of CO_2 escaping, through the pellet, is slower than the one through the bed powders.[37] Both evidences lead to the experimental observation of Fig. 2. In our previous findings[38] we showed that a small amount of impurities in limestone rocks do not influence the dynamic thermal decomposition of pellet heated at 10 °C/min. Fig. 2 reproduces the same behaviour for the doped and non doped pellets. In the same figure the kinetic behaviour of doped and non doped powder is somewhat different. Since absorption–desorption step of CO_2 trough the powder packing bed might influence such a behaviour, let us to minimize this effect by reducing the amount of powder in the crucible and the heating rate.

Fig. 3 presents the dynamic TG traces of loose C and CD powders in air at an heating rate of 0.1 °C/min. It can be observed

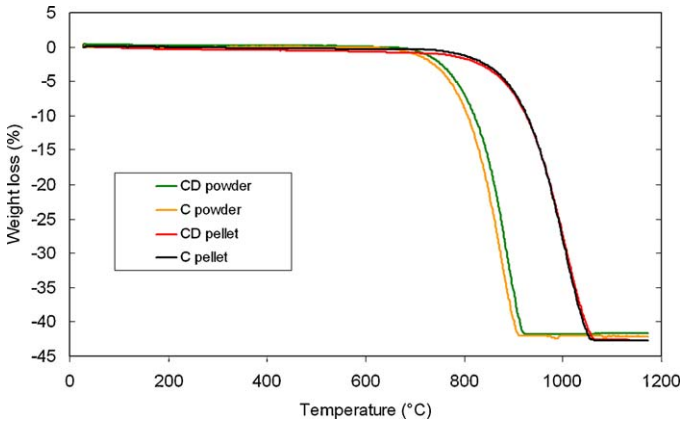

Fig. 2. Typical dynamic TG traces of loose C and CD powders and their correspondent pellets exhibiting an apparent density of 1.89–1.91 g/cm^3 and decomposed in air and at a heating rate of 10 °C/min.

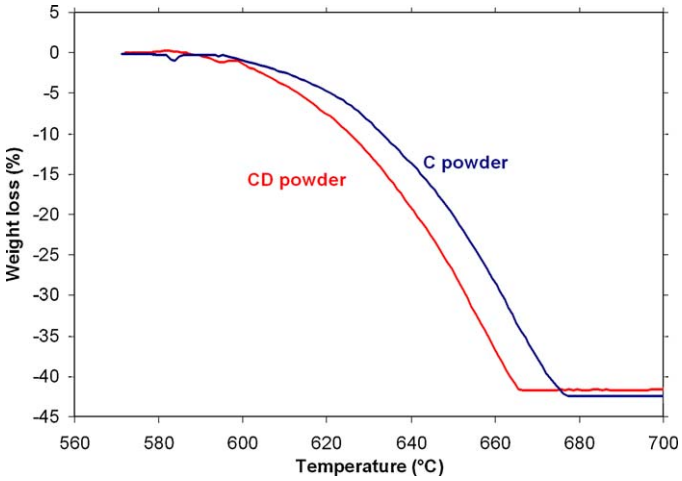

Fig. 3. Typical dynamic TG traces of loose C and CD powders in air at a heating rate of 0.1 °C/min.

that the heating rate influences the kinetics of decomposition of loose C and CD powders; both powders start to decompose at the same temperature of 590 °C, but Al^{3+} ions enhance the rate of CD powder decomposition.

Fig. 4 illustrates the weight loss (%) during the thermal decomposition of C and CD pellets (see Fig. 2) and the total $\Delta L/L_0$ linear shrinkage traces of equivalent pellets in the dilatometer and with the same heating rate and gaseous environment.

As done in our recent paper,[39] we divided the dilatometer traces into three arbitrary regions. The first one (I) between 25 and 590 °C is the region where no decomposition of calcium carbonate occurs. In the second region (II) between 590 and 1150 °C, calcium carbonate decomposes. In this temperature range, a number of steps occur: nucleation and growth of CaO, interactions of Al^{3+} ions with CaO and/or $CaCO_3$ diffusion of the CO_2 through the formed porous CaO and sintering catalyses by the escaping gas among the formed oxide grains.[12] As a result of these different steps, the actual sample length of the C and CD samples will be a balance among the different contributions. The third and last region, III, is influenced by densification of CaO grains, grain growth and eventually reaction to form mixed oxides when the Al^{3+} ions are present. No differences were observed among the linear $\Delta L/L_0$ traces of the C and CD samples in region I. However, when the samples reached the temperature at which $CaCO_3$ decomposition begins (590 °C), the CD trace proceeded for a while along the linear line, whereas the C trace declined. As a reduction of $\Delta L/L_0$ is expected when the decomposition starts, evidently, the Al^{3+} ions interacted with the nascent CaO of the doped particles to reduce this effect.

Furthermore, the shrinkage of the C pellets was greater than that of the CD samples until the end of decomposition, although the CD particles exhibited a faster decomposition rate as demonstrated by the TG experiments at 0.1 °C/min. Thus, the effects of Al^{3+} ions endure throughout the entire decomposition-sintering stage.

Fig. 5 shows the IR pure powder spectra of CD and C pellets completely decomposed in air at 900 °C and then prepared for the FT-IR measurements at room temperature through an heating period under vacuum at 400 °C to eliminate possible hydration compounds. For the C sample, above the cutoff of the pure powder at 600 cm^{-1}, several components can be detected at 713 and 874 cm^{-1} (sharp) and at 1074 and 1120 cm^{-1} (shoulder) that can be assigned to vibrational modes of carbonate groups at the surface in different coordination states.[40]

Correspondingly, the broad and strong absorption (to saturation of the signal) in the 1300–1600 cm^{-1} region is due to carbonate stretching modes. At high frequencies, the band at 3650 cm^{-1} is due to OH stretching modes of residual Ca–OH groups.

The addition of Al^{3+} ions to the calcium carbonate material permits the detection of additional components at 749, 768, 908, 973 and 996 (broad and weak) cm^{-1} that can be assigned to the cation-oxygen vibrational modes of AlO_4 groups. As previously discussed by other authors,[41] bands in this region suggest the diffusion of aluminium ions into NaCl-type oxides

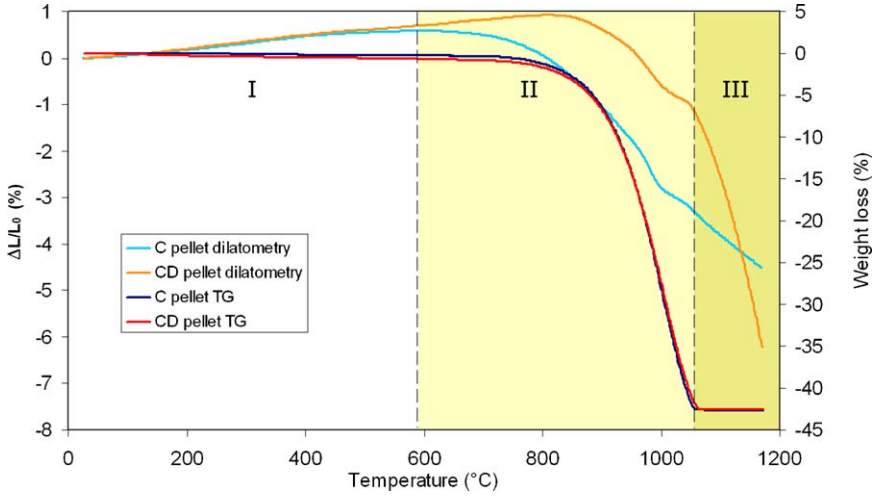

Fig. 4. Weight loss (%) during the thermal decomposition of C and CD pellets and total $\Delta L/L_0$ linear shrinkage traces of equivalent pellets in the dilatometer with the same heating rate and gaseous environment.

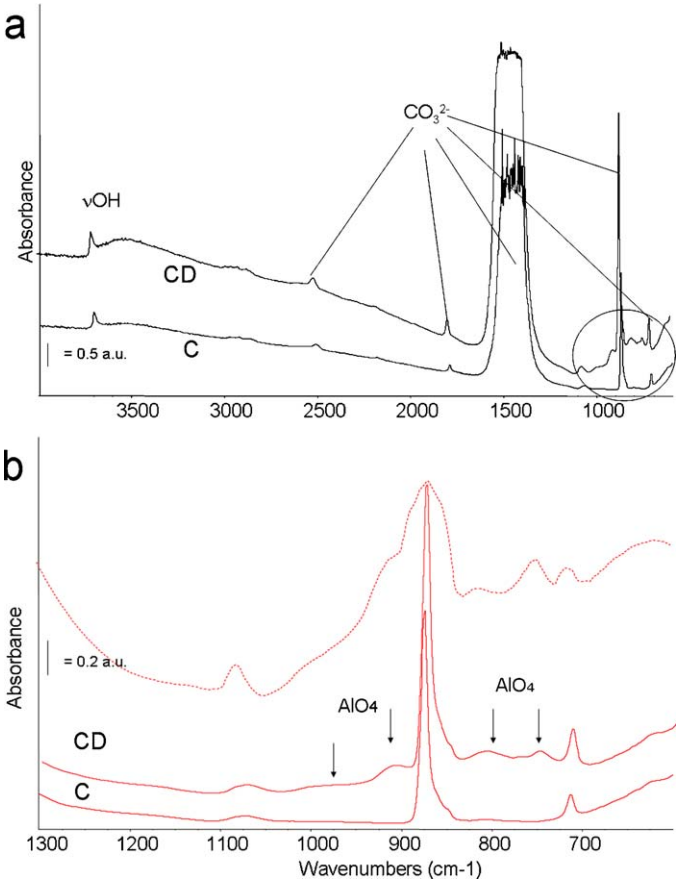

Fig. 5. (a) Pure powder FT-IR spectra of C and CD samples following outgassing at 400 °C. (b) Enlargement of the low-frequency region. Broken line spectrum: skeletal FT-IR subtraction spectrum [CD sample] − [C sample].

in a similar manner to Ni–Al oxides at the tetrahedral sites of cubic oxygen packing. These aluminate groups can be located just below the external oxide surfaces in amounts that can be revealed by the FT-IR techniques but not by XRD techniques.[41] The FT-IR traces of C and CD calcium carbonate pellets (see Supplementary Fig. 1) do not exhibit the presence of AlO_4 groups.

By coupling the FT-IR results with the dilatometer results, it can be concluded that the differences in the thermal dilation curves of the C and CD pellets in region II are due to the diffusion of the Al^{3+} ions into CaO.

This process enhances the decomposition of the $CaCO_3$ particles, but it reduces the rate at which the pellets formed by $CaCO_3$/CaO shrink.

Fig. 6 shows SEM images of CaO produced from C and CD carbonate decomposition in air at 900 °C (a and b) or heated at 900 °C in air for 1 h (c and d). By comparing these images with those of the starting carbonates particles, it can be said that the carbonate decomposition in air is a pseudomorphic process; the CaO grains form a porous network,[11] and the doped CaO grains are larger than the undoped grains. The doped samples shrink less than not doped ones (see Fig. 7), but their specific surface values are going in the opposite direction: 11 m^2/g with additive, versus 15 m^2/g, w/o additive.

Coarsening and densification (i.e. sintering) are two competitive phenomena in the reduction of surface area and in the increase of relative density,[38] the above evidences clearly suggest that in the doped sample the coarsening step is prevalent. If so Al^{3+} diffuses in the CaO grains enhancing the ion surface mobility that leads to a greater coarsening.

Fig. 7 shows the dilatometer traces of the C and CD pellets that decomposed completely in air at 950 °C. They prove that the linear shrinkage of the doped samples at the end of the isothermal heating (see point Q) is less than that of the undoped specimens (see point P). It is interesting to observe that at the end of the decomposition period, in the absence of the escaping CO_2 molecules but in the presence of the CO_2 molecules present in the air, the isothermal heating treatments at 950 °C for 8 h produced further sintering in the undoped CaO network but had no effect on the shrinkage of the doped oxide. Accordingly, the specific surface area of the not doped samples decreased from 15 to 13 m^2/g, whereas that of the doped sample remained at 11 m^2/g.

This last experimental observation is an anticipation of the dilatometer data reported in Fig. 8.

The traces are relevant to C and CD pellets decomposed in the dilatometer at 950 °C in CO_2 flux and then heated for 8 h under the same conditions. In the same figure, for the sake of comparison, the dilatometer curves of equivalent samples that decomposed in air are reported. The presence of a CO_2 flux over the samples decreased the final porosity of the undoped oxides from 67 to 62% but increased that of the doped oxides from 64 to 66%.

Based on these results and as far as the temperature range of 590–950 °C is concerned, we can conclude that the diffusion of Al^{3+} ions in the tetrahedral interstitial sites of CaO promotes the coarsening of the oxide grains. Then, from the dilatometer data in air and in CO_2 flux, we can infer that the AlO_4 groups might reduce the catalytic effect of CO_2 on the sintering of oxides. However, the coarsening phenomena that we have demonstrated appear independent from the presence of CO_2 molecules in the gaseous environment, and any coarsening phenomenon reduces the rate of the shrinkage. Thus, it is unclear that the coarsening effect due to the Al^{3+} ions is associated with a reduction of the catalytic action of CO_2.

To escape from this dilemma, it is necessary to know the ultimate mechanism according to which the CO_2 catalyses the sintering of CaO.

In our previous study,[42] we demonstrated that CO_2 adsorbs chemically in the temperature range of 650–930 °C on the O^{2-} surface sites of CaO to form CO_3^{2-} ions for a degree of coverage that ranges from 55 to 99%. When the surface area reaches a high degree of coverage, the CO_3^{2-} ions diffuse into CaO through a grain boundary path. In contrast with this behaviour, CO_2 adsorbs onto MgO surfaces, forming complex carbonate species that do not penetrate in their bulk phases.[26,42] Because CO_2 is more efficient in catalysing the CaO grains than the MgO grains, it was postulated that for an agent in its gaseous phase to catalyse the sintering of a ceramic oxides, it must both adsorb chemically at the oxide surface and diffuse into the oxide.[27]

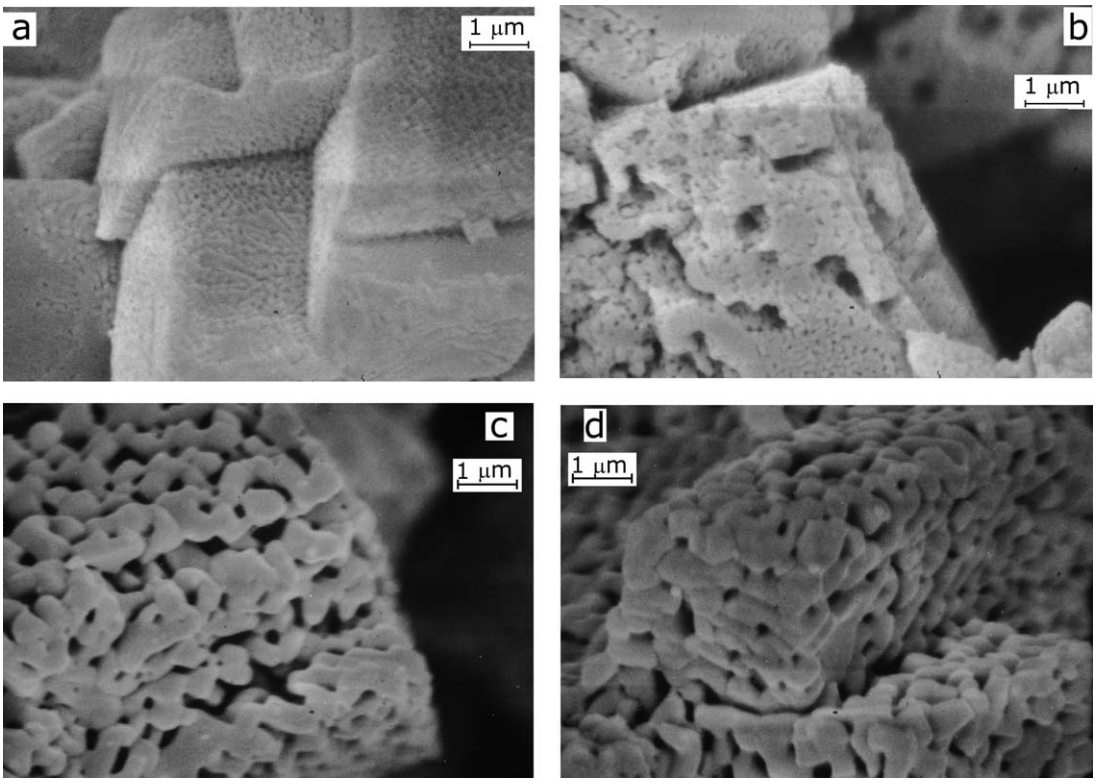

Fig. 6. SEM images (11,000×) of CaO produced from C and CD carbonate decomposition in air at 900 °C (a and b) and then heated at 900 °C in air for 1 h (c and d).

If that postulate is correct, then the Al^{3+} ions must reduce the penetration of the CO_3^{2-} ions in CaO "via" grains boundaries.

Fig. 9 illustrates the equilibrium adsorption–desorption isotherms measured when CO_2 adsorbs onto undoped and doped calcium oxide at the temperature of 728 °C and at a pressure below the CO_2 equilibrium carbonation pressure. The increase of the slope where the final adsorption points of curve I adjusts implies that there is penetration of CO_3^{2-} ions into CaO.[42]

As demonstrated by curve red, the uptake of CO_2 to form CO_3^{2-} ions is lower for doped CaO than for undoped CaO because the formation of AlO_4 groups reduces the number of O^{2-} surface sites available to CO_2 in the undoped oxide. Furthermore, the final slope of isotherm red is less than that of curve blue, and thus, the penetration of CO_3^{2-} ions into doped CaO through grain boundaries is reduced.

As an important conclusion, these data establish that Al^{3+} ions are linked to the CO_2 uptake as well as decrease this uptake. Consequently, they reduce the catalytic effect of CO_2 on CaO sintering. This effect is additive with the natural reduction in the sintering rate they catalyse due to their coarsening effect.

The behaviour of the dilatometer curves in region III (see Fig. 2) clearly reveals that the effect of the Al^{3+} ions is temperature-dependent. At temperatures exceeding 1000 °C, the

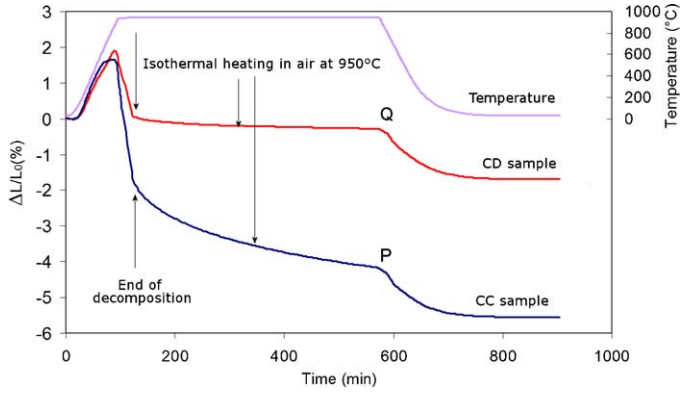

Fig. 7. Typical dilatometer traces of the C and CD pellets decomposed completely in air at 950 °C for 8 h.

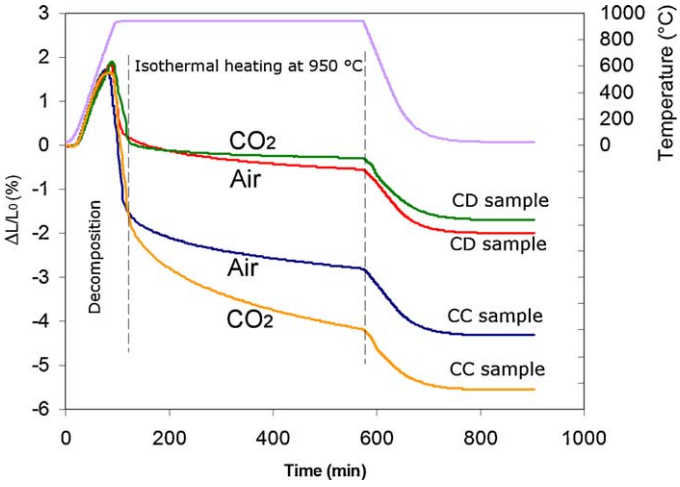

Fig. 8. Comparison of typical dilatometer traces of the C and CD pellets decomposed completely in CO_2 flux at 950 °C for 8 h and the equivalent samples decomposed in air.

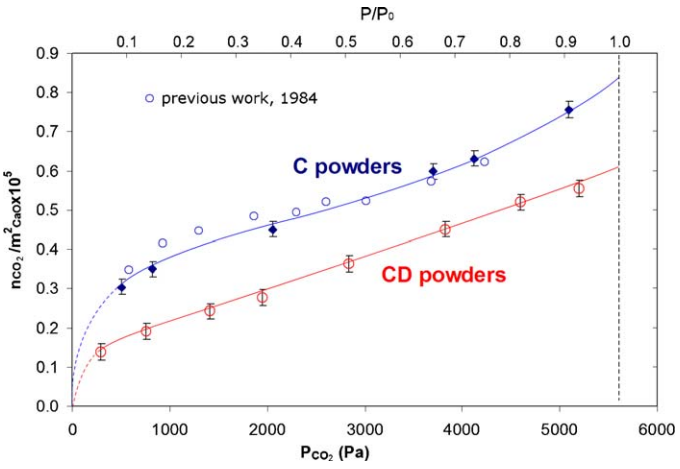

Fig. 9. Equilibrium adsorption–desorption isotherms of CO_2 at 720 °C and pressures below the CO_2 equilibrium carbonation pressure for CaO produced from C (upper curve) and CD (lower curve) carbonate decomposition in air at 900 °C. The round empty symbols in the upper curve are referred to experimental values of a previous work.[42]

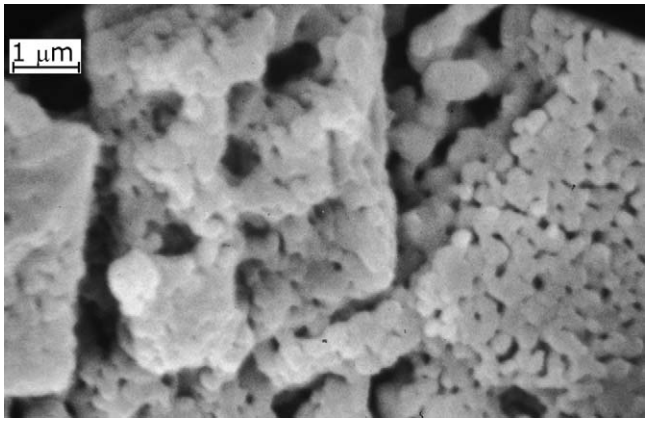

Fig. 10. SEM images (11,000×) of CaO produced from CD carbonate decomposition in air at 1050 °C.

rate of shrinkage of the doped sample increases dramatically. SEM observations of doped CaO particles treated in air at 1050 °C (see Fig. 10) indicate that there are very dense spots and less dense spots on the external visible surfaces. The enhanced sintering rate might be due to viscous flow and/or sintering of the calcium aluminate phases.

The decarbonation/carbonation cycles are characterised by temperatures in the range of 700–950 °C when the looping solids are the limestone type.[1] This is a safe method to exploit the benefits of calcium oxides doped with Al^{3+} ions, but caution is required if higher temperatures are used.

4. Conclusions

The first scientific achievement of this paper is elucidating the mechanisms that govern the catalysis of CO_2 (g) during the sintering steps of CaO grains obtained by the thermal decomposition of $CaCO_3$ and/or exposed to CO_2 flux/atmosphere at temperatures exceeding 600 °C.

The rule that can be derived from this mechanism is that for gases such as CO_2 and H_2O to serve as catalysts of the sintering of ceramic oxides such as CaO and MgO, they must be both adsorbed chemically at the oxide surfaces and diffused into the oxide, probably through grain boundary paths.

A direct extension of this achievement is that in the $CaCO_3$ pseudomorphic decomposition reaction, the small nascent CaO interconnected grains exposed to the CO_2 flux undergo a more rapid sintering step than larger grains due to the high number of grain boundary paths.

The second scientific achievement of this paper is demonstrating how and why doping the starting $CaCO_3$ particles with Al^{3+} ions produces doped CaO that reduces its sintering rate when exposed to CO_2 flux below the equilibrium decomposition pressure in the temperature range of 590–1000 °C. For higher temperatures, this protection rapidly decreases.

Al^{3+} ions that diffuse into CaO form AlO_4 groups at the tetrahedral sites below the CaO grain surfaces. This promotes the coarsening of the oxide grains and reduces the number of O^{2-} sites on CaO surfaces. Consequently, minor amounts of CO_3^{2-} ions will be available to migrate in CaO, and this reduces its sintering rate.

This demonstrated mechanism can be a guideline to select others doping agents. On this basis, potential metallic ions should exhibit two characteristics: being smaller than Ca^{2+} to be able to diffuse into CaO interstitial sites and the ability to subtract O^{2-} ions from the surface of CaO to decrease the amount of CO_2 that can adsorb onto the surface of CaO. Metallic ions that are the same size as Ca^{2+} or larger are not expected to be promising due to their possibility of substituting for Ca^{2+}.

Acknowledgements

This work was financially supported by funds from DIChePresearch contracts. The authors wish to thank the Lhoist Recherche et Dèveloppement S.A. for his interest in this field of research. We thank Prof. G. Busca for the useful contribution in the interpretation of the IR results. We thank also D. Vitiello for technical help during his time in our laboratory in which he was preparing a B.A. thesis on some items developed and accomplished in this paper. One of the author, D.T.B. wishes to thank Prof. Alan W. Searcy, U.C. Berkeley, for the useful exchange of idea that he had during his recent visit at U.C.

Appendix A. Supplementary data

Supplementary data associated with this article can be found, in the online version, at doi:10.1016/j.jeurceramsoc.2011.08.022.

References

1. Salvador C, Lu D, Anthony EJ, Abanades JC. Enhancement of CaO for CO_2 capture in an FBC environment. *Chem Eng J* 2003;**96**:187–95.
2. Blamey J, Anthony EJ, Wang J, Fennell PS. The calcium looping cycle for large-scale CO_2 capture. *Prog Energy Combust Sci* 2010;**36**(2):260–79.

3. Ströhle J, Galloy A, Epple B. Feasibility study on the carbonate looping process for post-combustion CO_2 capture from coal-fired power plants. *Energy Proc* 2009;**1**(1):1313–20.
4. http://www.caoling.eu/.
5. Nayar A. The steel handbook. McGraw Hill; 2001.
6. Huijen WJJ, Comans RNJ. Carbonation of steel slag for CO_2 sequestration: leaching of products and reaction mechanism. *Environ Sci Technol* 2006;**40**:2790–6.
7. Daniele V, Taglieri G, Quaresima R. The nanolimes in cultural heritage conservation: characterization and analysis of the carbonation process. *J Cult Heritage* 2008;**9**(3):294–301.
8. Abanades JC, Anthony EJ, Lu DY, Salvador C, Alvarez D. Capture of CO_2 from combustion gases in a fluidised bed of CaO. *AIChE J* 2004;**50**:1614–22.
9. Fennel PS, Davidson JF, Dennis e JS, Hayhurst AN. Regeneration of sintered limestone sorbents for the sequestration of CO_2 from combustion and other systems. *J Energy Inst* 2007;**80**(2):116–8.
10. Ferrini V, De Vito C, Mignardi S. Synthesis of nesquehonite by reaction of gaseous CO_2 with Mg chloride solution: its potential role in the sequestration of carbon dioxide. *J Hazard Mater* 2009;**168**:832–7.
11. Erwing J, Beruto D, Searcy AW. The nature of CaO produced by calcite powders decomposition in vacuum and in CO_2. *J Am Ceram Soc* 1979;**62**:580.
12. Beruto D, Barco L, Searcy AW. CO_2-catlyzed area and porosity changes in high-surface-area CaO aggregates. *J Am Ceram Soc* 1984;**67**(7):512–5.
13. Borgwardt RH. Calcium oxide sintering in atmospheres containing water and carbon dioxide. *Ind Eng Chem Res* 1989;**28**:493–500.
14. Alvarez D, Abanades JC. Pore-size and shape effects on the recarbonation performance of calcium oxide submitted to repeated calcination/recarbonation cycles. *Energy Fuels* 2005;**19**:270–8.
15. Sun P, Grace JR, Lim CJ, Anthony EJ. The effect of CaO sintering on cyclic CO_2 capture in energy systems. *Environ Energy Eng* 2007;**53**(9): 2432–42.
16. Li ZS, Cai NS, Huang YY. Effect of preparation temperature on cyclic CO_2 capture and multiple carbonation–calcination cycles for a new Ca-based CO_2 sorbent. *Ind Eng Chem Res* 2006;**45**:1911–7.
17. Li ZS, Cai NS, Huang YY, Han HJ. Synthesis, experimental studies and analysis of a new calcium-based carbon dioxide sorbent. *Energy Fuels* 2005;**19**:1447–52.
18. Feng B, Liu WQ, Li X, An H. Overcoming the problem of loss-in-capacity of calcium oxide in CO_2 capture. *Energy Fuels* 2006;**20**:2417–20.
19. Gupta H, Fan LS. Carbonation–calcination cycle using high reactivity calcium oxide for carbon dioxide separation from flue gas. *Ind Eng Chem Res* 2002;**41**(16):4035–42.
20. Hughes RW, Lu D, Anthony EJ, Yu Y. Improved long-term conversion of limestone-derived sorbents for in situ capture of CO_2 in a fluidized bed combustor. *Ind Eng Chem Res* 2004;**43**(18):5529–39.
21. Aihara M, Nagai T, Matsushita J, Negishi YI, Ohya H. Development of porous solid reactant for thermal-energy storage and temperature upgrade using carbonation/decarbonation reaction. *Appl Energy* 2001;**69**:225–38.
22. Kimura S, Adachi M, Noda R, Horio M. Particle design and evaluation of dry CO_2 recovery sorbent with a liquid holding capability. *Chem Eng Sci* 2005;**60**:4061–71.
23. Manovic V, Anthony EJ. Steam reactivation of spent CaO-based sorbent for multiple CO_2 capture cycles. *Environ Sci Technol* 2007;**41**(4):1420–5.
24. Manovic V, Anthony EJ. Long-term behavior of CaO-based pellets supported by calcium aluminate cements in a long series of CO_2 capture cycles. *Ind Eng Chem Res* 2009;**48**(19):8906–12.
25. Pacciani R, Muller CR, Davidson JF, Dennis JS, Hayhurst AN. Synthetic Ca-based solid sorbents suitable for capturing CO_2 in a fluidized bed. *Can J Chem Eng* 2008;**28**:356–66.
26. Beruto DT, Botter R, Searcy AW. H_2O catalyzed sintering of ~2-nm-cross-section particles of MgO. *J Am Ceram Soc* 1987;**70**(3):155–9.
27. Beruto DT, Searcy AW, Botter R, Giordani M. Thermodynamics and kinetics of H_2O (v) chemisorption and solubility in nanometric and single-crystal MgO particles during sintering. *J Phys Chem* 1993;**97**:9201.
28. Reed JS. Introduction to principles of ceramic processing. second ed. New York, USA: John Wiley & Sons; 1995.
29. Powder Diffraction File. Joint committee on powder diffraction standards. Swarthmore, PA: International Centre for Diffraction Data; 1991 [Card No. 5-0586].
30. Blazek A. Thermal analysis. New York: Van Nostrand Reinhold; 1972. p. 25.
31. Beruto D, Searcy AW. Use of Langmuir method for kinetic studies of decomposition reactions: calcite ($CaCO_3$). *J Chem Soc Faraday Trans* 1974;**1**(70):2145–53.
32. Hills AW. The mechanism of thermal decomposition of calcium carbonate. *Chem Eng Sci* 1968;**23**:297–320.
33. Beruto D, Kim MG, Searcy AW. The kinetics of decomposition in powders beds: theory and experiment, U.C. Preprint-16069 (1983) and 163rd Electrochem Soc Meeting. "High Temperature materials chemistry - II".
34. Stern KH, Weise EL. High temperatures properties and decomposition of inorganic salts, part 2, carbonates. Washington, DC: National Bureau of Standards; 1969.
35. Beruto DT, Barco L, Belleri G, Searcy AW. Vapor-phase hydration of submicrometer CaO particles. *J Am Ceram Soc* 1981;**64**(2):74–80.
36. Florin NH, Blamey J, Fennel PS. Synthetic CaO-based sorbent for CO_2 capture from large-point sources. *Energy Fuels* 2010;**24**(8):4598–604.
37. Beruto DT, Searcy AW, Kim MG. Microstructure, kinetic, thermodynamic analysis for calcite decomposition: free surface and powder bed experiments. *Thermochim Acta* 2004;**424**:99–109.
38. Lange FF. Densification of powder compacts: an unfinished story. *J Eur Ceram Soc* 2008;**28**:1509–16.
39. Beruto DT, Botter R, Cabella R, Lagazzo A. A consecutive decomposition-sintering dilatometer method to study the effect of limestone impurities on lime microstructure and its water reactivity. *J Eur Ceram Soc* 2010;**30**(6):277–86.
40. Busca G, Lorenzelli V. Infrared spectroscopic identification of species arising from reactive adsorption of carbon oxides on metal oxide surfaces. *Mater Chem* 1982;**7**(1):89–126.
41. Resini C, Montanari T, Barattini L, Ramis G, Busca G, Presto S, et al. Hydrogen production by ethanol steam reforming over Ni catalysts derived from hydrotalcite-like precursors: catalyst characterization, catalytic activity and reaction path. *Appl Catal A: Gen* 2009;**355**(1–2):83–9.
42. Beruto DT, Searcy AW, Botter R. Thermodynamics and kinetics of carbon dioxide chemisorption on calcium oxide. *J Phys Chem* 1984;**88**:4052–5.